Supplemental Material of "Half-Metallic *p*-Type $LaAlO_3/EuTiO_3$ Heterointerface from Density Functional Theory"

Hai-Shuang Lu,[1] Tian-Yi Cai,[1] Sheng Ju,[1,*] and Chang-De Gong[2,3,†]

[1] *Department of Physics and Jiangsu Key Laboratory of Thin Films, Soochow University, Suzhou 215006, P. R. China*

[2] *Center for Statistical and Theoretical Condensed Matter Physics and Department of Physics, Zhejiang Normal University, Jinhua 321004, P. R. China*

[3] *National Laboratory of Solid State Microstructure and Department of Physics, Nanjing University, Nanjing 210093, P. R. China*

[*] Email address: jusheng@suda.edu.cn

[†] Email address: cdgongsc@nju.edu.cn

First, we provide the supporting materials (I-VI) of our main calculations based on GGA+U with $U = 4$ eV, including the structure properties of all superlattices and the electronic band structure of the *nn*-type and the *pp*-type superlattices.

I. Table I for the total energies of the *nn*-type and the *pp*-type digital heterostructures with various magnetic orderings.

II. Table II for the optimized lattice constant for the *nn*-type and the *pp*-type digital heterostructures.

III. Figure 1 for the electronic band structure of the *nn*-type digital heterostructures, including 3-2, 4-2, 5-2, 4-3 and 5-3.

IV. Figure 2 for the electronic band structure of the *pp*-type digital heterostructures, including 3-1, 4-1 and 5-1.

V. Table III for the total energies of the *np*-type digital heterostructures with various magnetic orderings.

VI. Table IV for the optimized lattice constant for the *np*-type digital heterostructures.

Second, we demonstrate the Hubbard U dependence of the magnetic and electronic properties of the bulk $EuTiO_3$ (VII) and the calculations of superlattices with an alternative Hubbard U of 3 eV (VIII-XI).

VII. Table V for the Hubbard U dependence of the total energies of the bulk $EuTiO_3$ and the corresponding transition temperatures. The magnetic exchange couplings between neighboring Eu ions are derived from the total energies of various magnetic orderings and the transition temperature is obtained within mean field theory. It is found that with increasing the Hubbard U, the antiferromagnetic coupling is weakened. When U reaches as high as 5 eV, the ferromagnetic ordering becomes the ground state. However, when U is less than 3 eV, $EuTiO_3$ becomes metallic. Regarding the fact that the experimental observed Néel temperature of the bulk $EuTiO_3$ is around 5.5 K and the insulating nature of $EuTiO_3$, it can be concluded that U of around 4 eV is a reasonable choice for $EuTiO_3$ [1, 2]. To show the situation when the Hubbard U is decreased, in the following we have also shown the calculations based on U of 3 eV, where the ferromagnetic ordering in the *nn*-type

superlattices, the half-metallic electronic state in the *pp*-type superlattices, and a magnetic ordering driven insulator-to-metal transition with the coexistence of fully spin-polarized electrons and holes in the *np*-type superlattices are also found.

VIII. Table VI for the total energies (meV per Eu) of the *nn*-type and the *pp*-type digital heterostructures with various magnetic orderings. Here, $U = 3$ eV.

IX. Figure 3 for the electronic density of state of the *nn*-type 4-3 and the *pp*-type 4-1 digital heterostructures. Here, $U = 3$ eV.

X. Figure 4 for the electronic band structure of the *nn*-type 4-3 digital heterostructure. Here, $U = 3$ eV.

XI. Figure 5 for the electronic band structure of the *pp*-type 4-1 digital heterostructure. Here, $U = 3$ eV.

XII. Table VII for the total energies of the *np*-type digital heterostructures with various magnetic orderings. Here, $U = 3$ eV.

XIII. Figure 6 for the electronic band structure of the *np*-type digital heterostructures of 2-1 and 3-1. Here, $U = 3$ eV. The magnetic ordering driven insulator-to-metal transition is also found. In addition, for these superlattices within the FM ordering, the unique band structure also supports the coexistence of the fully spin-polarized electrons and holes as revealed in the context with U of 4 eV.

XIV. Figure 7 for the electronic band structure of the *np*-type digital heterostructures of 3-2 and 4-2. Here, $U = 3$ eV. Clearly, in both AFM and FM states, the systems are metallic. Clearly, compared with the calculations based on the U of 4 eV, the differences agree with the fact that the band gap of pristine $EuTiO_3$ is reduced when the U changes from 4 eV to 3 eV.

Third, we demonstrate the effect of the Hubbard U at Ti sites. Both the bulk $EuTiO_3$ (XV) and the superlattices (XVI-XXI) are studied. For the bulk $EuTiO_3$, the inclusion of the Hubbard U on the Ti $3d$ orbitals will overestimate the FM coupling, leading to a FM ground state. This result is in disagreement with the experimentally observed G-type AFM ordering. For the *nn*-type superlattice and the *pp*-type superlattice, the inclusion of the Hubbard U at Ti site does not change the main results. The negatively spin-polarized Ti $3d$ orbitals in the *nn*-type systems and the half-metallic nature in the *pp*-type systems are

still found. For the *np*-type superlattice, the inclusion of the Hubbard U at Ti site will increase the band gap between the Eu $4f$ and Ti $3d$ orbitals a little. The evolution of the band structure associated with the zigzag potential in these polar-non-polar digital superlattices do not change.

XV. Table VIII for the Hubbard U (on Ti $3d$ orbital) dependence of total energies of bulk $EuTiO_3$. Clearly, when a Hubbard U is applied on the Ti $3d$ orbitals, the FM ordering becomes the ground state, which does not agree with the experimental finding.

XVI. Table IX shows the total energies of the *nn*-type 4-3 superlattice with different U on the Ti $3d$ orbital.

XVII. Figure 8 shows the electronic state of the *nn*-type 4-3 superlattice with different U on the Ti $3d$ orbital.

XVIII. Table X shows the total energies of *pp*-type 4-1 superlattice with different U on the Ti $3d$ orbital.

XIX. Figure 9 shows the electronic state of the *pp*-type 4-1 superlattice with different U on the Ti $3d$ orbital.

XX. Table XI shows the total energies of the *np*-type superlattices. Here, the U is 1 eV for the Ti $3d$ orbital.

XXI. Figure 10 shows the electronic state in the *np*-type superlattices. Here, the U is 1 eV for the Ti $3d$ orbital.

Finally, we use the experimental lattice constant of 3.905 Å for $SrTiO_3$ substrate as the in-plane lattice constant to study the electronic and magnetic properties of $LaAlO_3/EuTiO_3$ superlattices. We can find that the main results do not change.

XXII. Table XII shows the magnetic ordering dependence of the total energies of the *nn*-type 4-3 superlattice and the *pp*-type 4-1 superlattice with an in-plane lattice constant of 3.905 Å. Clearly, the FM ordering is still the ground state for both *nn*-type and *pp*-type superlattices.

XXIII. Figure 11 shows the electronic state of the *nn*-type 4-3 superlattice and the *pp*-type 4-1 superlattice with an in-plane lattice constant of 3.905 Å. The negatively spin-

polarized Ti 3d states in the nn-type superlattice and the half-metallic nature in the pp-type superlattice do not change.

XXIV. Table XIII shows the energy difference between the FM state and the AFM state in the np-type superlattices with an in-plane lattice constant of 3.905 Å. The optimized lattice constants along c axis are also shown.

XXV. Figure 12 shows the electronic state of the np-type superlattices with an in-plane lattice constant of 3.905 Å.

TABLE I: Total energies (meV per Eu) of the *nn*-type and the *pp*-type digital heterostructures with various magnetic orderings.

	nn 3-2	*nn* 4-2	*nn* 5-2	*nn* 4-3	*nn* 5-3	*pp* 3-1	*pp* 4-1	*pp* 5-1
FM	**0**	**0**	**0**	**0**	**0**	**0**	**0**	**0**
G-type AFM	6.24	6.69	6.66	3.85	3.83	6.47	4.99	99.71
A-type AFM	–	–	–	2.79	2.77	10.89	9.20	9.15
C-type AFM	–	–	–	3.71	3.77	10.93	12.03	110.59

TABLE II: The optimized lattice constant for the *nn*-type and the *pp*-type digital heterostructures.

	nn 3-2	*nn* 4-2	*nn* 5-2	*nn* 4-3	*nn* 5-3	*pp* 3-1	*pp* 4-1	*pp* 5-1
c (Å)	11.67	15.40	19.13	15.62	19.35	11.32	15.05	18.79

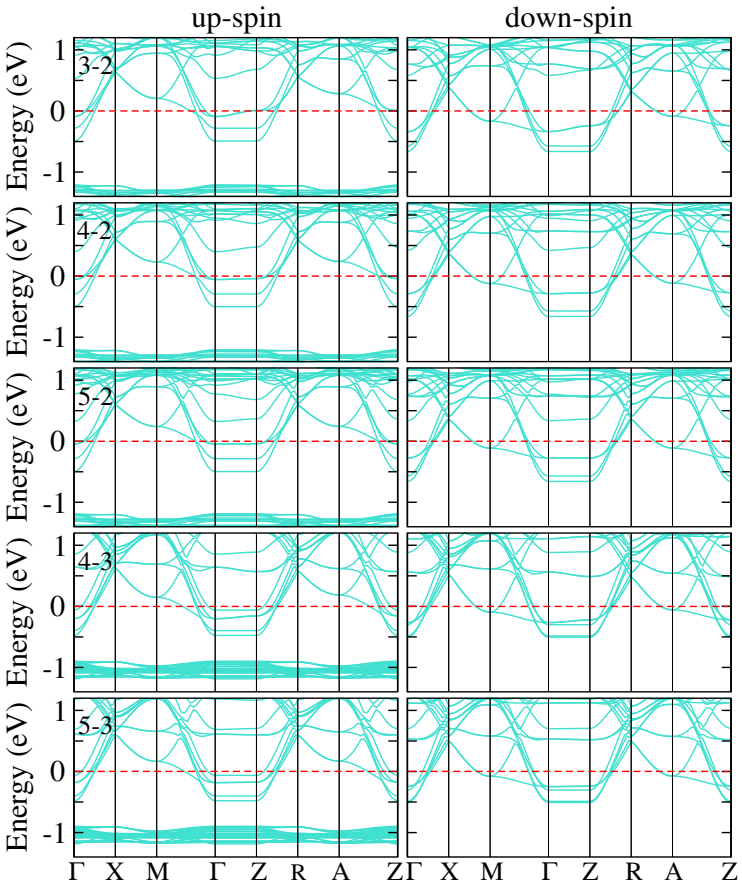

FIG. 1: **Electronic band structure of the *nn*-type digital heterostructures, including 3-2, 4-2, 5-2, 4-3 and 5-3. Normal ferromagnetic state is found in all the cases. The Fermi level is at energy zero with dashed line.**

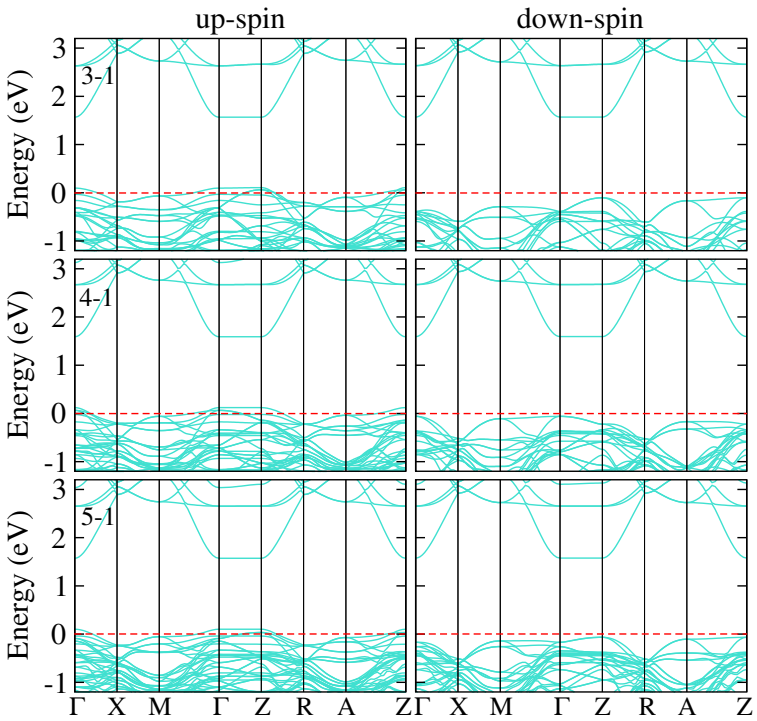

FIG. 2: **Electronic band structure of *pp*-type digital heterostructures, including 3-1, 4-1 and 5-1. Half-metallic state is found in all the cases. The Fermi level is at energy zero with dashed line.**

TABLE III: Total energies (meV per Eu) of the *np*-type digital heterostructures with various magnetic orderings.

	2-1	3-1	4-1	5-1	3-2	4-2	5-2
FM	0.21	0.55	0.7	0.81	**0**	**0**	**0**
G-type AFM	**0**	**0**	**0**	**0**	0.30	0.32	0.43
A-type AFM	–	–	–	–	0.98	0.86	0.82
C-type AFM	–	–	–	–	0.90	0.88	1.00

TABLE IV: Optimized lattice constant for the *np*-type digital heterostructures.

	2-1	3-1	4-1	5-1	3-2	4-2	5-2
c (Å)	7.68	11.42	15.16	18.89	11.64	15.39	19.14

TABLE V: The Hubbard U (eV) dependence of total energies of bulk $EuTiO_3$ (meV per Eu) for various magnetic orderings, the estimated transition temperature (T_N or T_C (K)), and the corresponding electronic state in the ground state.

U	0	1	2	3	4	5	6
E (FM)	4.618	4.248	3.440	2.183	0.763	**0**	**0**
E (G-type AFM)	**0**	**0**	**0**	**0**	**0**	0.355	0.980
E (A-type AFM)	8.053	7.423	5.728	3.840	2.008	1.055	0.940
E (C-type AFM)	8.940	6.975	5.310	3.828	2.410	1.598	1.415
T_N or T_C	26.84	23.16	17.98	12.24	6.43	3.74	2.89
Metal or Insulator	Metal	Metal	Metal	Insulator	Insulator	Insulator	Insulator

TABLE VI: Total energies (meV per Eu) of *nn*-type and *pp*-type digital heterostructures with various magnetic orderings. Here, $U = 3$ eV.

	nn 3-2	*nn* 4-2	*nn* 5-2	*nn* 4-3	*nn* 5-3	*pp* 3-1	*pp* 4-1	*pp* 5-1
FM	**0**	**0**	**0**	**0**	**0**	71.22	**0**	**0**
G-type AFM	11.00	7.03	7.00	5.06	4.12	**0**	3.01	2.85
A-type AFM	–	–	–	3.10	3.07	84.03	11.48	11.20
C-type AFM	–	–	–	4.60	4.68	5.15	15.02	14.68

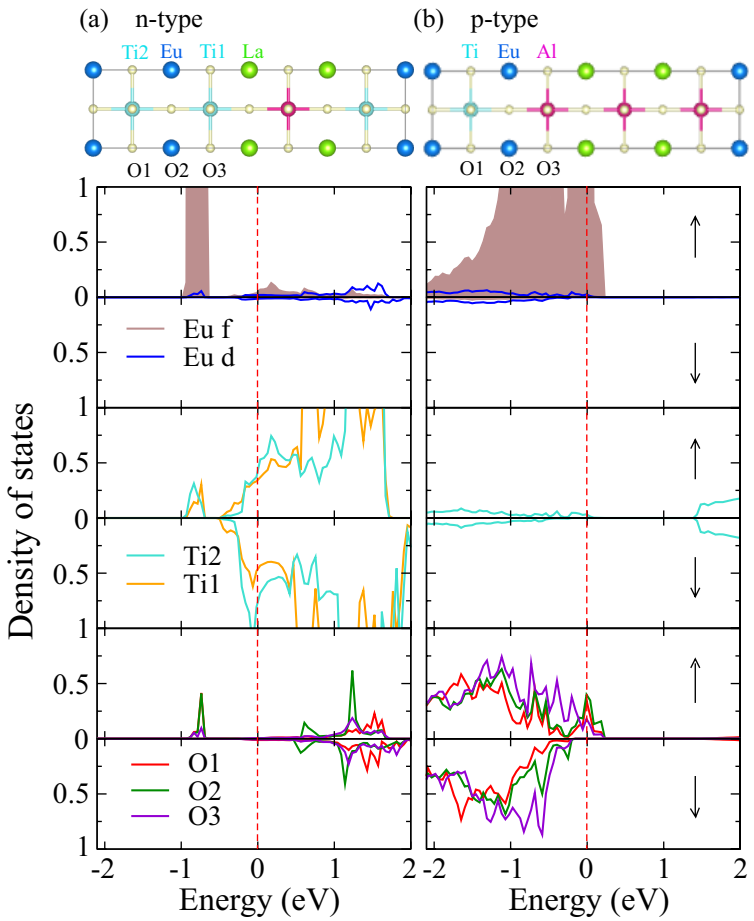

FIG. 3: **(a) Up panel: Illustration of symmetric *nn*-type 4-3 $LaAlO_3/EuTiO_3$ digital heterostructure. Down panel: Partial density of states in *nn*-type 4-3. (b) Up panel: Illustration of symmetric *pp*-type 4-1 $LaAlO_3/EuTiO_3$ digital heterostructure. Down panel: Partial density of states in *pp*-type 4-1. The Fermi level is at energy zero with dashed line indicated. Here, $U = 3$ eV.**

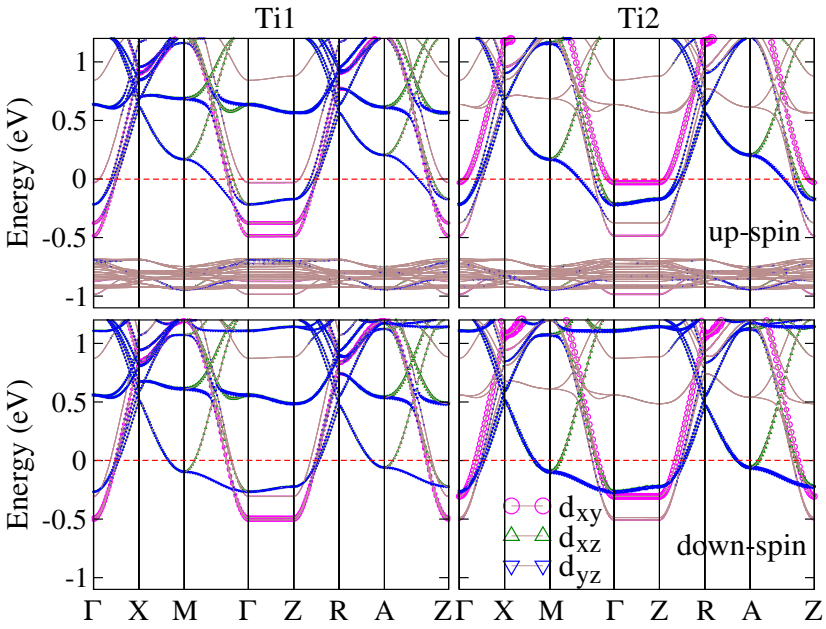

FIG. 4: **Orbital resolved band structure of nn-type 4-3. The Fermi energy is set to zero. Here, $U = 3$ eV and the system is normal ferromagnet.**

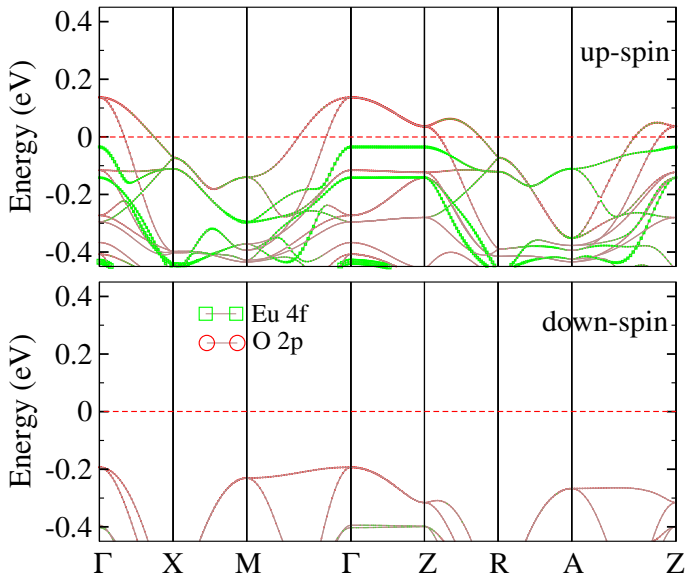

FIG. 5: **Orbital resolved band structure of *pp*-type 4-1. The Fermi energy is set to zero. Here, $U = 3$ eV and system is half-metallic.**

TABLE VII: Total energies (meV per Eu) of *np*-type digital heterostructures with various magnetic orderings. Here, $U = 3$ eV.

	FM	G-type AFM	C-type AFM	A-type AFM
2-1	1.57	**0**	–	–
3-1	**0**	1.52	–	–
4-1	**0**	1.68	–	–
5-1	**0**	1.21	–	–
3-2	0.71	**0**	1.03	1.61
4-2	0.45	**0**	0.87	0.91
5-2	0.37	**0**	0.92	1.47

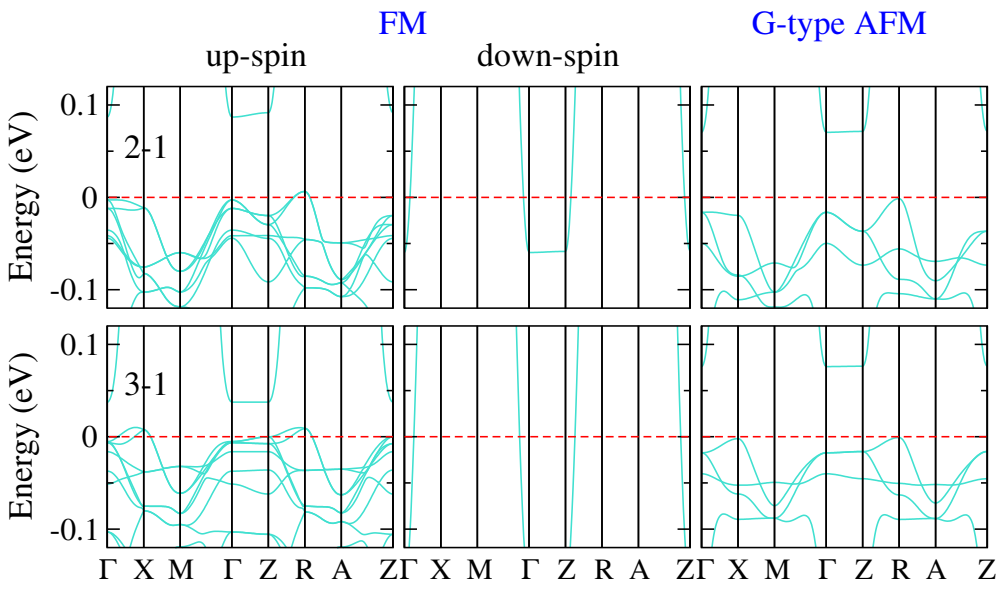

FIG. 6: **Electronic density of states of np-type 2-1 and 3-1. The Fermi energy is set to zero. Here, $U = 3$ eV.**

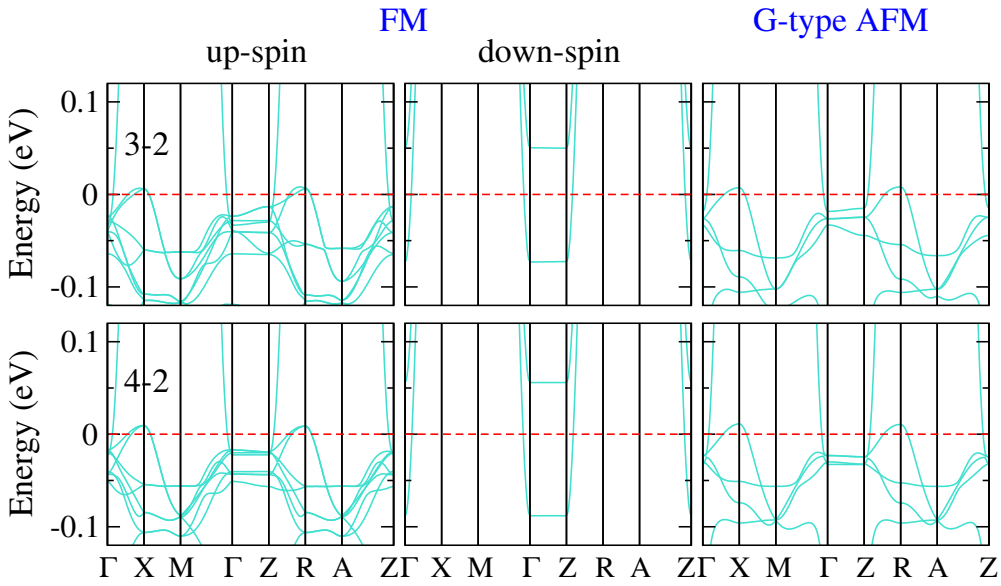

FIG. 7: **Electronic density of states of np-type 3-2 and 4-2. The Fermi energy is set to zero. Here, $U = 3$ eV.**

TABLE VIII: Total energies of $EuTiO_3$ bulk with different Hubbard U on the Ti $3d$ orbital. Here, the value of U on the Eu $4f$ electrons is still 4 eV. Clearly, when the Hubbard U is applied at the Ti site, the bulk $EuTiO_3$ becomes FM, which is in disagreement with experimental findings.

U (eV)	1	2	3
FM	**0**	**0**	**0**
A-type AFM	1.693	2.000	2.195
C-type AFM	2.140	2.478	2.693
G-type AFM	0.068	0.708	1.198

TABLE IX: Magnetic ordering dependence of the total energies (meV/Eu) in the *nn*-type 4-3 superlattice with different Hubbard U on the Ti $3d$ orbital. Here, the value of the Hubbard U on the Eu $4f$ orbital is still 4 eV.

	FM	A-type AFM	C-type AFM	G-type AFM
$U = 1$ eV	**0**	4.00	5.05	5.09
$U = 2$ eV	**0**	7.75	8.98	8.90
$U = 3$ eV	**0**	13.74	15.03	14.83

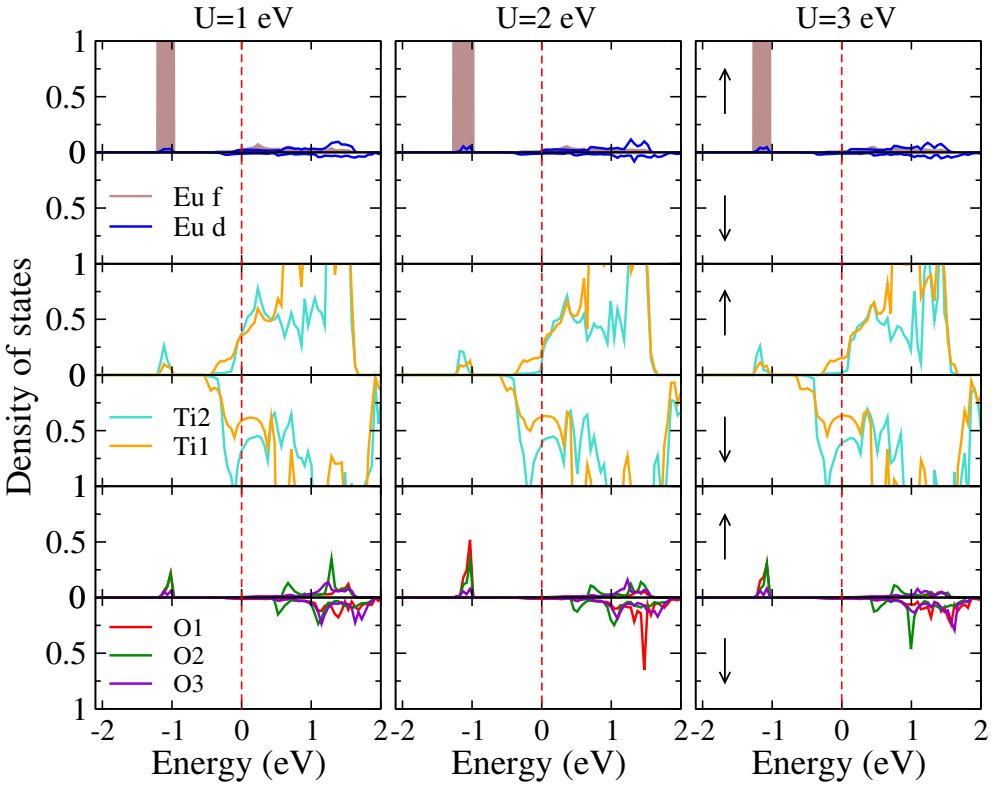

FIG. 8: **Electronic density of states of *nn*-type 4-3 superlattice with different Hubbard U on the Ti $3d$ orbital. Here, the value of the Hubbard U on the Eu $4f$ orbital is still 4 eV. The Fermi energy is set to zero.**

TABLE X: Magnetic ordering dependence of the total energies (meV/Eu) in the *pp*-type 4-1 superlattice with different Hubbard U on the Ti $3d$ orbital. Here, the value of the Hubbard U on the Eu $4f$ orbital is still 4 eV.

	FM	A-type AFM	C-type AFM	G-type AFM
$U = 1$ eV	**0**	9.11	12.05	5.02
$U = 2$ eV	**0**	9.02	12.06	5.02
$U = 3$ eV	**0**	8.92	12.03	5.02

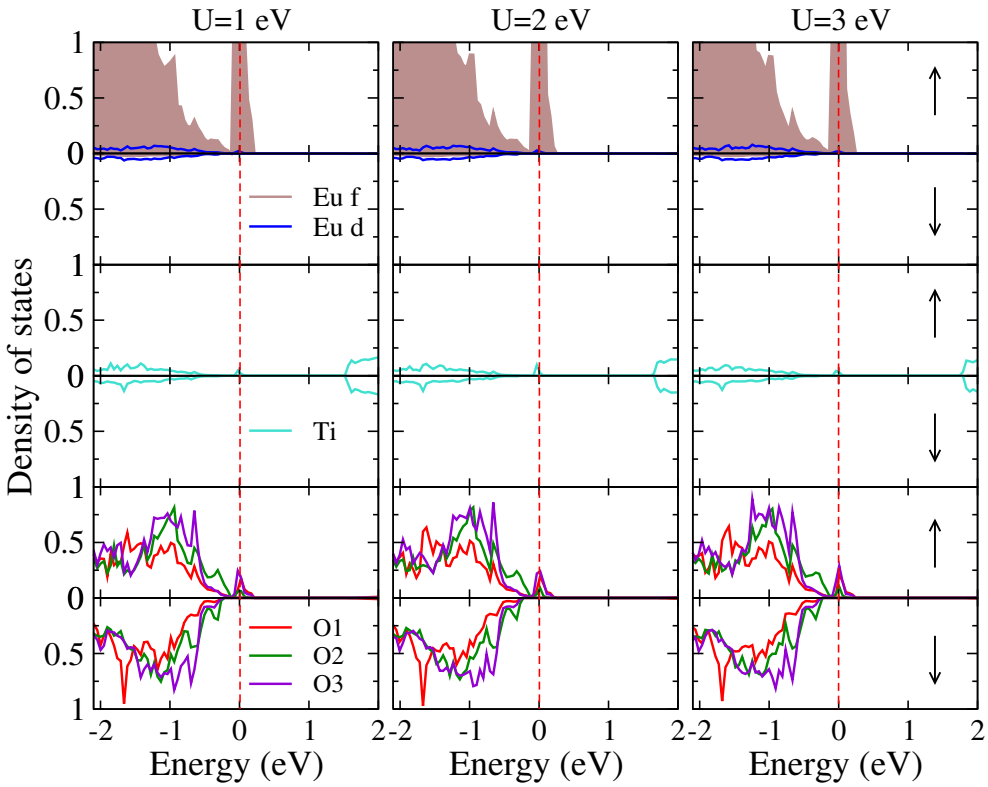

FIG. 9: **Electronic density of states of *pp*-type 4-1 superlattice with different Hubbard U on the Ti $3d$ orbital. Here, the value of the Hubbard U on the Eu $4f$ orbital is still 4 eV. The Fermi energy is set to zero.**

TABLE XI: Energy difference between the G-type AFM state and the FM state ($\Delta E = E_{AFM} - E_{FM}$ (meV/Eu)) in the np-type superlattices. Here, the Hubbard U on the Ti $3d$ orbitals is 1 eV and the U on the Eu $4f$ orbital is still 4 eV.

	2-1	3-1	4-1	5-1	3-2	4-2	5-2
ΔE	0.38	0.17	0.05	-0.05	0.80	0.82	0.86

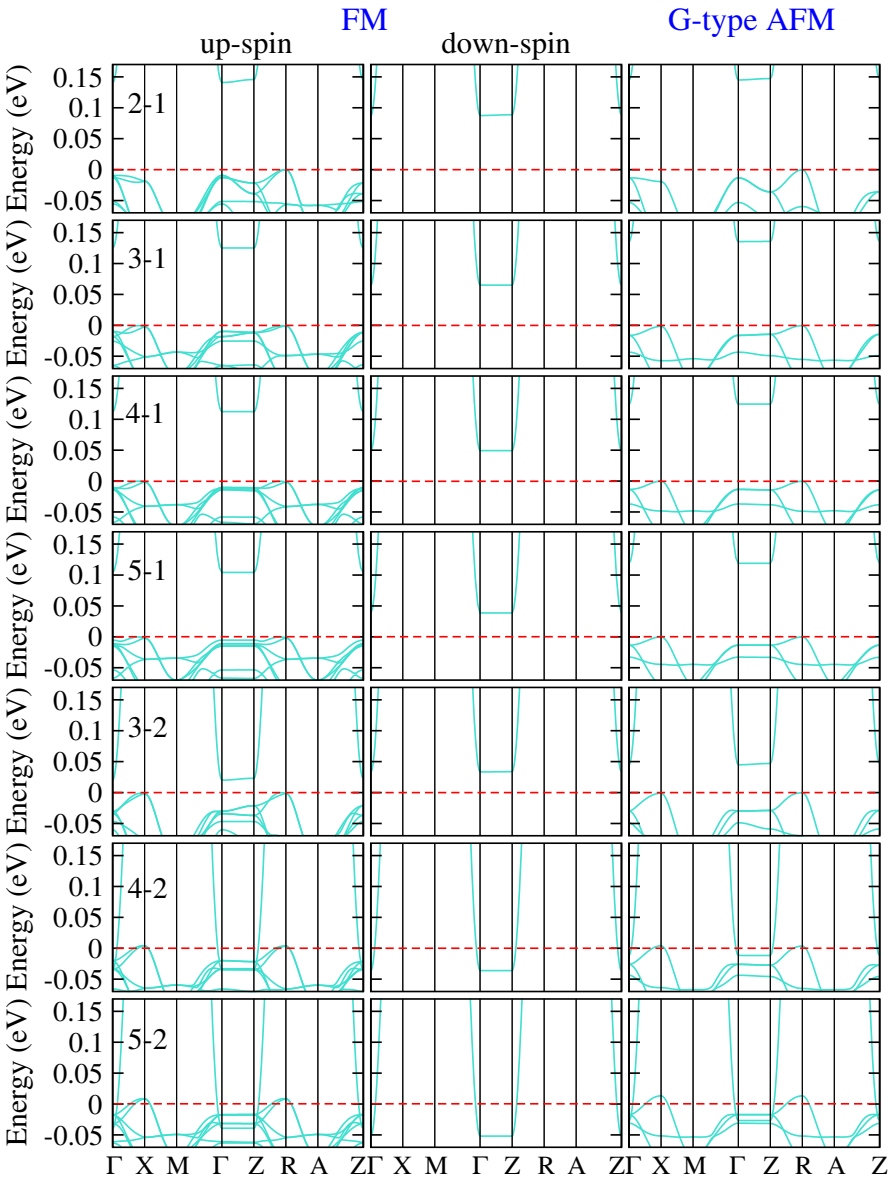

FIG. 10: **Electronic density of states of the np-type superlattices. Here, the Hubbard U is 1 eV for Ti $3d$ orbitals and the U on the Eu $4f$ orbitals is still 4 eV. The Fermi energy is set to zero.**

TABLE XII: Total energies (meV/Eu) of the *nn*-type 4-3 superlattice and the *pp*-type 4-1 superlattice. Here, the in-plane lattice constant is 3.905 Å, which is the experimental value of $SrTiO_3$ substrate. The optimized lattice constant along *c* axis is 15.75 Å and 15.15 Å for the *nn*-type 4-3 superlattice and the *pp*-type 4-1 superlattice, respectively.

	FM	A-type AFM	C-type AFM	G-type AFM
nn-type 4-3	**0**	3.22	3.72	4.47
pp-type 4-1	**0**	8.71	111.73	100.68

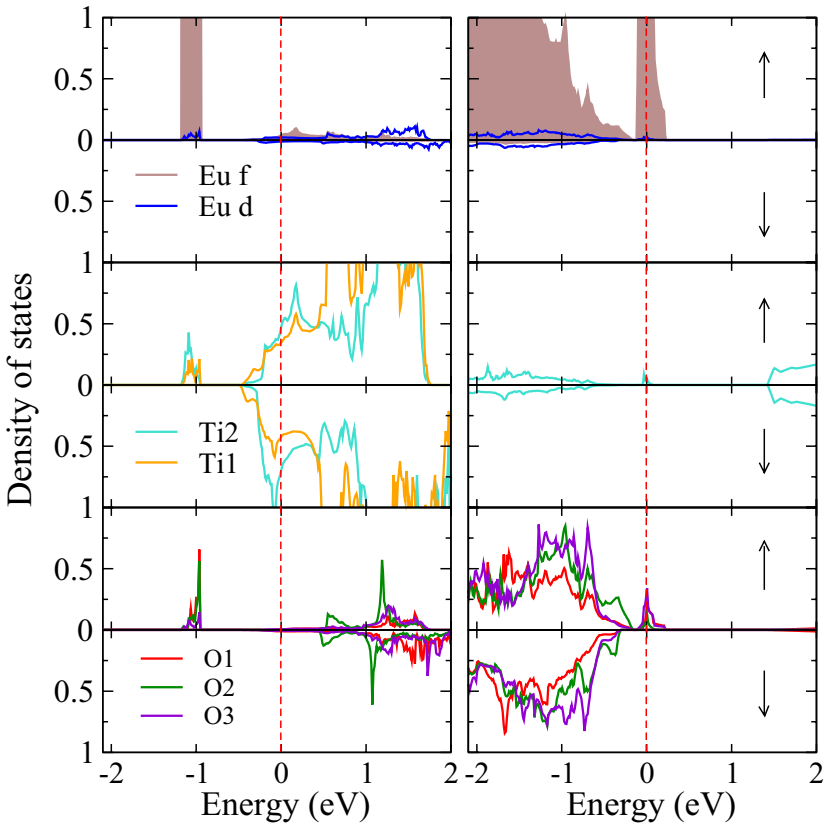

FIG. 11: **Electronic density of states of nn-type 4-3 superlattice (left) and *pp*-type 4-1 superlattice (right). Here, the in-plane lattice constant is 3.905 Å, which is the experimental value of $SrTiO_3$ substrate. The Fermi energy is set to zero.**

TABLE XIII: The energetics and the lattice constant (c axis) of the np-type superlattices. Here, the in-plane lattice constant is 3.905 Å, which is the experimental value of $SrTiO_3$ substrate. $\Delta E = E_{AFM} - E_{FM}$.

	2-1	3-1	4-1	5-1
ΔE (meV/Eu)	0.11	-0.19	-0.18	0.19
c (Å)	7.74	11.50	15.30	19.05

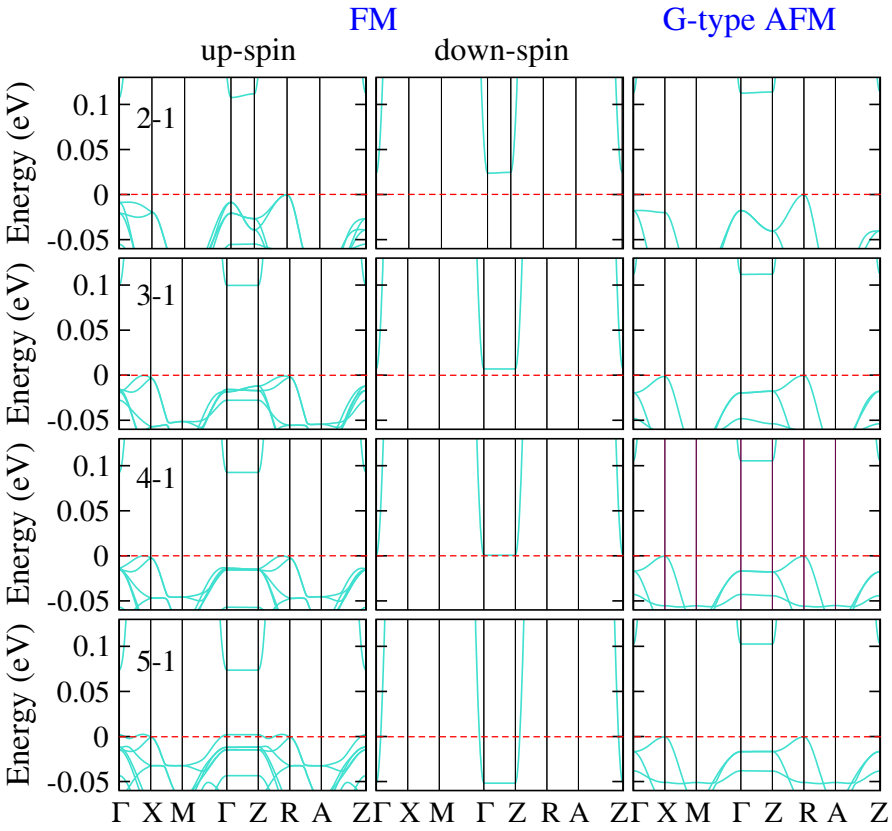

FIG. 12: **Evolution of the electronic band structure of the *np*-type $LaAlO_3/EuTiO_3$ superlattices. Here, the in-plane lattice constant is 3.905 Å, which is the experimental value of $SrTiO_3$ substrate. The Fermi energy is set to zero.**

[1] C. J. Fennie and K. M. Rabe, Magnetic and electric phase control in epitaxial $EuTiO_3$ from first principles, Phys. Rev. Lett. **97**, 267602 (2006).

[2] Y. Yang, W. Ren, D. Wang, and L. Bellaiche, Understanding and revisiting properties of $EuTiO_3$ bulk material and films from first principles, Phys. Rev. Lett. **109**, 267602 (2012).